Measurement 218 (2023) 113250

Contents lists available at ScienceDirect

Measurement

journal homepage: www.elsevier.com/locate/measurement

Direct interface circuits for resistive sensors affected by lead wire resistances

José A. Hidalgo-López

Departamento de Electrónica, Universidad de Málaga, Málaga 29071, Spain

ARTICLE INFO

Keywords:
Remote sensor
Resistive sensor
Sensor interface electronics
Time-based measurement

ABSTRACT

This article proposes two novel circuits for the digital readout of resistive sensors with parasitic series resistances caused by the lead wire needed to connect remote sensors. Both circuits are based on so-called direct interface circuits (DICs). These circuits perform a resistance-to-time-to-digital conversion by adding some external components to a digital processors (DP). The new circuits are very simple since they only use a capacitor and two or three resistors, depending on the proposal. A single discharging of the capacitor provides two or three time measurements to estimate the resistance of the sensor, eliminating the influence of lead wire resistances. Using a single discharging process simultaneously reduces error sources, measurement time, and energy consumption. A circuit that uses an FPGA as DP to estimate resistances corresponding to several thermal sensors presents systematic errors below 0.15% or 0.12%, depending on the proposal, for a maximum measurement time of 1.09 ms.

1. Introduction

The Internet of Things (IoT) conceives a world where smart physical objects are connected to form a global network. These smart objects acquire data about their existing state or their surrounding environment [1,2]. Therefore, the sensors that provide these data are fundamental to IoT. In an IoT node, the information produced by the sensors is usually read by a digital processor (DP) through an interface circuit. Accordingly, an adequately designed IoT node requires an efficient interface circuit that allows a direct sensor-DP connection with few components, reading the sensor information quickly and with as little power consumption as possible.

These are precisely the characteristics found in so-called direct interface circuits (DICs). DICs allow a sensor-DP connection via a magnitude-to-time-to-digital conversion that does not require analog-to-digital converters (ADC). A few components perform the magnitude-to-time conversion, while the DP carries out the time-to-digital conversion. The magnitude-to-time conversion can only use passive components or, at most, some operational amplifiers (OA) and switches, but always in very limited numbers. DICs can be used to read resistive sensors [3–5], capacitive sensors [6–8], and inductive sensors [9].

One of the most widely used physical variables in IoT is temperature, both in industrial and environmental applications. Thanks to their behavior, resistance temperature detectors (RTD) have become one of the most popular sensors for temperature measurement. Unfortunately, the distance from the sensor to the signal conditioning circuit in some applications requires a long-range lead wire. This implies having two parasitic series resistors connected to the RTD. These lead wire resistances, R_{w1} and R_{w2}, may also be temperature dependent.

Several proposals to avoid the distortion introduced by lead wire resistances in reading an RTD can be found in the literature. One relatively common idea is to use two diodes connected directly to the sensor, as shown in Fig. 1, where the sensor is modeled by a resistor, R_X. Circuit operation requires V_{in} to be measured when a current, I_{in}, is made to flow in the direction shown in Fig. 1. The current's direction is then changed (maintaining its magnitude) and V_{in} is remeasured. The sum of the two voltages, ΣV_{in}, is

$$\Sigma V_{in} = I_{in}R_X + (V_{D1} - V_{D2}) \tag{1}$$

where V_{D1} and V_{D1} are the voltages across diodes D_1 and D_2, respectively, when they are forward-biased. If I_{in} and ΣV_{in} are known, and the diodes are a perfect match, then R_X can be obtained as

$$R_X = \frac{\Sigma V_{in}}{I_{in}} \tag{2}$$

With some modifications, this technique repeatedly appears in the literature. The method was initially proposed in [10], where two OAs, four additional resistors, and an ADC are used in addition to the diodes. However, no data on errors in the R_X estimation are provided. More complex circuits are introduced in [11,12] where, in addition to an ADC,

E-mail address: jahidalgo@uma.es.

https://doi.org/10.1016/j.measurement.2023.113250
Received 15 March 2023; Received in revised form 20 June 2023; Accepted 23 June 2023
Available online 26 June 2023

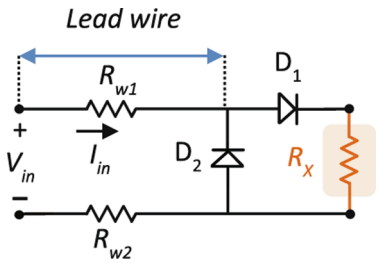

Fig. 1. Circuit with two diodes to reduce errors in reading the resistive sensors due to the resistance of the lead wires.

a variable number of OAs, switches, resistors, and other elements are needed. Despite the complexity of the circuits, the errors are 1.96% for a Pt1000 in [11] and 0.98% for a Pt100 in [12]. Based on a circuit similar to that of Fig. 1 [13,14] perform a resistance-to-time conversion with different active and passive components in the interface circuit but without ADC. In [13], errors of 0.86% are reported for R_X in a range of 100–1000 Ω, while in [14], the errors are 0.24% plus a hysteresis of 0.59% in a reduced range of 100–150 Ω.

A slightly different technique for a resistance-to-time conversion [15] uses a single diode and a resistor near the sensor instead of two diodes. The circuit needs two switches, an OA, three voltage references, and an additional resistor showing an error of 0.87% for resistive sensors in the range of 100–180 Ω. [16] also uses a single diode but in this case, a Zener. This proposal needs a voltage source, a current source, switches, and resistors. Error is 0.24% with R_X in the 848–2120 Ω range.

Most of the errors in these proposals relate to the fact that closely matched diodes are not possible for discrete devices (it is shown in [17] that a minimum difference of 1 mV between V_{D1} and V_{D2} translates to a 0.5% error for an RTD-Pt100). In addition, the currents in the two steps must also match perfectly, which requires complex circuitry.

With fewer components, DIC-based implementations have been proposed to offset lead wire resistance effects. The DIC in [17] uses three resistors, a capacitor, three switches, two diodes, and a microcontroller as DP (the microcontroller needs an analog comparator and a reference voltage). The reading method consists of three capacitor charging-discharging processes, obtaining three time measurements (performed during discharge) that provide the R_X estimate. Apart from the errors produced by the mismatch between the diodes, the accuracy of the estimation depends on the closeness of R_X to the value of a calibration resistor. That is why the results are only provided for a very narrow range of 100–146 Ω, limiting the usability of the circuit.

A different concept is developed in [18,19], using the so-called three-wire technique to obtain R_X. In this technique, a resistive sensor terminal is connected to a single lead wire, while the other is connected to two lead wires. The method only works if two lead wires connected to different terminals have the same resistance value. In [18], two switches, two resistors, a capacitor, two comparators, and a programmable gain amplifier are used to obtain the three time measurements to calculate the R_X estimation with errors up to 1.5%, but over a wide range of 1 kΩ – 1 MΩ. The circuit in [19] is simpler, consisting of four switches, five resistors, a capacitor, and a comparator. Three time measurements are also needed to obtain R_X; the error can reach 1.15% in this case.

The three-wire technique is also used in the DIC proposed in [20]. The circuit uses three additional resistors and a capacitor, with a microcontroller as the DIC, to get four time measurements (each obtained in a capacitor charging-discharging process) to estimate sensor resistance. Errors are 0.4 Ω for a resistance value of 50–300 Ω.

It is important to note that the DICs in [17–20] require multiple charging-discharging processes, which lengthens the time needed to estimate R_X. In addition, the voltages charged in the capacitors must be the same at the end of each charging process to ensure the correct operation of the circuits. In practice, this is difficult to achieve due to the noise in the circuit. Finally, [18–20] need three wires to connect the remote resistive sensor to the DP.

In this article, we propose two new DICs to reduce the effects of lead wire resistances on estimating a resistive sensor. The interface circuits only need two wires to connect the sensor and a few passive components. Besides, time measurements are obtained during a single charging-discharging process. All of this reduces measurement time, power consumption, and DP resource utilization. Despite the proposals' simplicity, the errors align with the lowest found in the literature.

2. Operating principles of the new proposals

2.1. Description and analysis of the two-measurement method

The first proposed DIC is shown in Fig. 2. This circuit is the main element of what we will call the *Two-Measurement Method*, TMM. The circuit consists of two resistors, R_A and R_B, and a capacitor, C, physically connected to the sensor side. The capacitor must be NP0 type and selected with a temperature coefficient equal to zero, as is possible in this kind of capacitor. The DP has no analog elements and only requires the P_A and P_B pins to be configurable as inputs (equivalent to high impedance state, HZ) or outputs. For the sake of simplicity, it is assumed that the output voltage levels are V_{DD} (the supply voltage of the DP) for the logical 1 output and 0 V for the logical 0 output.

The processes necessary to obtain an estimate of R_X are similar to those described in [8] (where a DIC for the measurement of capacitive sensors is presented that also uses two resistors of known value). As in [8], only two time measurements are needed to estimate the magnitude of the sensor. The steps to obtain R_X with the TMM are shown in Table 1. In the first step, the capacitor is charged by selecting P_A and P_B as outputs with $P_A = P_B = '1'$ for a time T_{ch}, as shown in Fig. 3. It is important to note that the maximum voltage stored in the capacitor in this step, $\Delta V_{Cap,\max}$, is always less than V_{DD} due to the voltage drop across R_{w1}, R_{w2}, and the output resistance of pins P_A or P_B, *ro*. In general, R_{w1}, R_{w2}, and *ro* are low, and the difference between $\Delta V_{Cap,\max}$, and V_{DD} is not very large. As shown below, it is not necessary to know the value of $\Delta V_{Cap,\max}$ to estimate R_X (or, equivalently, the *ro* value is irrelevant). In either case, at the end of the first step, $V_{DD} > V_A > V_B$, as shown in Fig. 3. However, the single most crucial thing to ensure the correct operation of the circuit is that V_A, $V_B > V_{TL}$, where V_{TL} is the threshold voltage to detect a logical 0 input in the P_A or P_B pins, starting from a logical 1 input level. Therefore, the P_A and P_B pins detect a logical '1' from the start of the discharging process (this situation is shown in Fig. 3).

In the second step, the P_A and P_B pins are configured as inputs (HZ) at the instant we consider time reference $t = 0$, and the capacitor is discharged through an equivalent resistor, R_T

$$R_T = (R_A + R_B + R_w) \parallel R_X \tag{3}$$

where $R_w = R_{w1} + R_{w2}$.

As $V_A > V_B$ during this discharging process, and there will be an

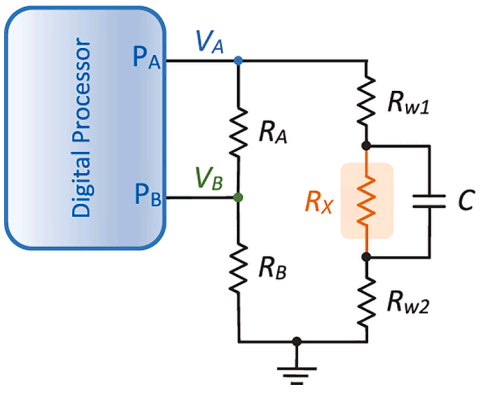

Fig. 2. Proposed circuit for the Two-Measurement Method (TMM).

TABLE 1
Steps to obtain R_X in the TMM.

STEPS	STATE OF PINS	
	P_A	P_B
1 – Charging C	'1'	'1'
2 – Discharging C	'HZ'	'HZ'

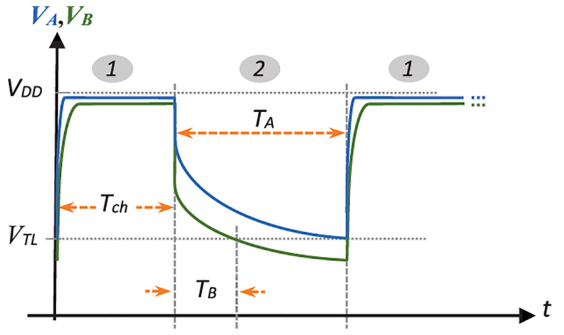

Fig. 3. $V_A(t)$ and $V_B(t)$ in the TMM circuit of Fig. 1 with the steps of Table I.

instant at which $V_B(t) = V_{TL}$, i.e., the detection instant of node B, T_B, see Fig. 3. Afterwards, there will be a detection instant for node A, T_A, also shown in Fig. 3. Since T_A and T_B are the two time measurements needed to estimate R_X, a new charging process can be started for a new measurement after obtaining T_A.

T_A and T_B are measured in an RC discharging circuit, so it is trivial to show that these times are

$$T_A = R_T C \ln\left(\frac{V_A(0)}{V_{TL}}\right) = R_T C \ln\left(\frac{\Delta V_{Cap,\max} - I(0)\cdot R_w}{V_{TL}}\right) \tag{4}$$

$$T_B = R_T C \ln\left(\frac{V_B(0)}{V_{TL}}\right) = R_T C \ln\left(\frac{R_B}{R_A + R_B}\cdot\frac{\Delta V_{Cap,\max} - I(0)\cdot R_w}{V_{TL}}\right) \tag{5}$$

where $I(0)$ is the current flowing through the capacitor when the discharging process begins. From (4) and (5), it is possible to obtain R_T as:

$$R_T = \frac{T_A - T_B}{C\cdot\ln\left(\frac{R_A+R_B}{R_B}\right)} = k(T_A - T_B) \tag{6}$$

being the value of k

$$k = \frac{1}{C\cdot\ln\left(\frac{R_A+R_B}{R_B}\right)} \tag{7}$$

Since the designer chooses C, R_A, and R_B, k is a known constant that can be stored in the DP.

As (3) shows, R_T does not match R_X; however, R_A and R_B can be set arbitrarily high such that $R_A + R_B \gg R_w$. In this case, we can obtain an approximate estimation of R_X, R_X*

$$R_X^* \approx \frac{1}{\frac{1}{R_T} - \frac{1}{R_A+R_B}} = \frac{k(R_A+R_B)(T_A - T_B)}{R_A + R_B - k(T_A - T_B)} \tag{8}$$

where R_T has been replaced by the result found in (6).

The TMM performs the steps shown in Table 1 for the circuit in Fig. 2, obtaining two time measurements, T_A and T_B, used in (8) to estimate R_X.

Relative error when using R_X* as an estimation of R_X can be found via simple arithmetic operations:

$$\frac{R_X^* - R_X}{R_X} = \frac{R_w}{R_A + R_B + R_w}\cdot\frac{R_X}{R_X + R_A + R_B} \tag{9}$$

This expression shows that the relative error is around zero if the designer chooses $R_A + R_B \gg R_w$, regardless of the value of R_X. Fortunately, the R_w values are, at most, in the order of a few tens of ohms. For example, lead wire resistance can vary between 0.2 Ω and 20 Ω, corresponding to the length of the 26 American wire gauge (AWG) lead wire from 1.5 m to 150 m (note that this is just an example, a cable of such dimensions also has significant inductive and capacitive effects). Values of the expression (9) of less than 0.1% are possible with R_A and R_B of the order of kilohms. Particularly interesting is the form of the second quotient of the right-hand term in (9), as it shows that relative error decreases as R_X decreases, a counter-intuitive situation.

The TMM could present a lower limit to the R_X values it can estimate. This is related to the fact, as mentioned, that $V_B(t = 0) > V_{TL}$ must be verified at the start of discharge or, equivalently.

$$V_B(0) = I(0)\cdot R_B = \frac{\Delta V_{Cap,\max}}{R_T}\cdot R_B > V_{TL} \tag{10}$$

But, as $\Delta V_{Cap,\max}$ decreases as R_X does, R_X cannot drop below a specific value. However, placing a low resistor in series with R_X across the capacitor terminals can easily overcome this limitation.

T_A - T_B must be increased to improve resolution in (6) and, therefore, in (8). This can be done by augmenting C; however, beyond a particular value, this does not increase the precision, as the uncertainty in the time measurement also rises, as will be shown later on. However, another way to increase T_A - T_B resolution is to modify the R_A/R_B ratio, making $V_B(0)$ slightly higher than V_{TL}, reducing T_B.

On the other hand, the errors in determining the values of R_A, R_B, and C will influence the accuracy of the estimates through the value of k. For this reason, it is important to use high-precision resistors and NP0 capacitors. In addition, it is convenient for capacitors to manually select these to guarantee the minimum changes of C due to temperature since, in an NP0 capacitor, these variations can oscillate between 0 and ±30 ppm/°C (which is less than ±0.3% change in C from −55 °C to +125 °C). In either case, effects such as hysteresis in the capacitor or changes in R_A, R_B, and C values over time can increase errors in R_X estimates.

Uncertainty in the time measurements, $u(T_A)$ and $u(T_B)$, contributes to increased errors in the R_X estimation. If the uncertainty caused by quantization in DP clock cycles of the time measurements is negligible, uncertainty is due mainly to the determination of trigger instant. This uncertainty, known as trigger uncertainty, $u_t(T)$, is inversely proportional to the slope of the discharge curve at the detection instant of V_A and V_B. Given this, in [8] it is found that $u(T_A)$ and $u(T_B)$ verify.

$$u(T_i) \approx u_t(T_i) = \frac{\alpha_i R_T C}{V_{TL}};\quad i = \{A, B\} \tag{11}$$

where α_i is a constant related to the noise voltage in the i node. Finally, from (6) and (11):

$$\frac{u(T_i)}{T_A - T_B} \approx \frac{\alpha_i}{V_{TL}\cdot\ln\left(\frac{R_A+R_B}{R_B}\right)};\quad i = \{A, B\} \tag{12}$$

Eq. (12) shows that time measurement quality does not depend on C, so it makes no sense to increase capacitance above a value that makes quantization effects negligible.

As relative uncertainty $u(R_X^*)/R_X^*$ is.

$$\frac{u(R_X^*)}{R_X^*} = \frac{1}{R_X^*}\sqrt{\left(\frac{\partial R_X^*}{\partial T_A}\right)^2 u^2(T_A) + \left(\frac{\partial R_X^*}{\partial T_B}\right)^2 u^2(T_B)}$$
$$\approx \sqrt{\left(\frac{u(T_A)}{T_A - T_B}\right)^2 + \left(\frac{u(T_B)}{T_A - T_B}\right)^2} \tag{13}$$

then, from (12).

$$\frac{u(R_X^*)}{R_X^*} \approx \frac{\sqrt{\alpha_A^2 + \alpha_B^2}}{V_{TL}\cdot\ln\left(\frac{R_A+R_B}{R_B}\right)} \tag{14}$$

In other words, relative uncertainty in estimating R_X* is practically

constant.

The value of α_i basically depends on two components [21]: a component resulting from the digital processor activity and a component due to interference superimposed on the supply voltage of the digital processor. In addition, [8,22] show that noise voltage in an RC discharge circuit is higher in the resistive node than in the capacitive node. This is due to the Johnson-Nyquist noise of the resistors and to the filtering effect of C. Thus, $\alpha_B > \alpha_A$ can be expected. This means that the T_A measurement is more precise than the T_B measurement and that the latter limits the precision of (8) as indicated by (14). These conclusions will be confirmed experimentally in Section III.

2.2. Description and analysis of the improved method

Fig. 4 (a) shows the modifications made to the circuit in Fig. 2 to improve the accuracy of the TMM. The circuit in Fig. 4 (a) is the main element in what we will call the *Improved Method*, IM. The main idea behind the IM is to take two measurements in resistive nodes of the RC discharge circuit that replace T_B in the TMM, such that $u(R_X^*)/R_X^*$ decreases.

For the time measurements to be similar in the TMM and the IM, the resistance value R_C should be the same as for R_B in the TMM, and $R_A + R_B$ in Fig. 4 (a) should take the same value as R_A in Fig. 3. The steps to follow to obtain the three time measurements required in the IM are shown in Table 2 (the new P_C pin in Fig. 4 (a) must also be a configurable input/output pin).

The waveforms in nodes A, B, and C of the IM circuit are shown in Fig. 4 (b). It is important to remember that R_A, R_B, and R_C have been chosen, so $V_C(t = 0) > V_{TL}$ ensures the correct operation of the circuit.

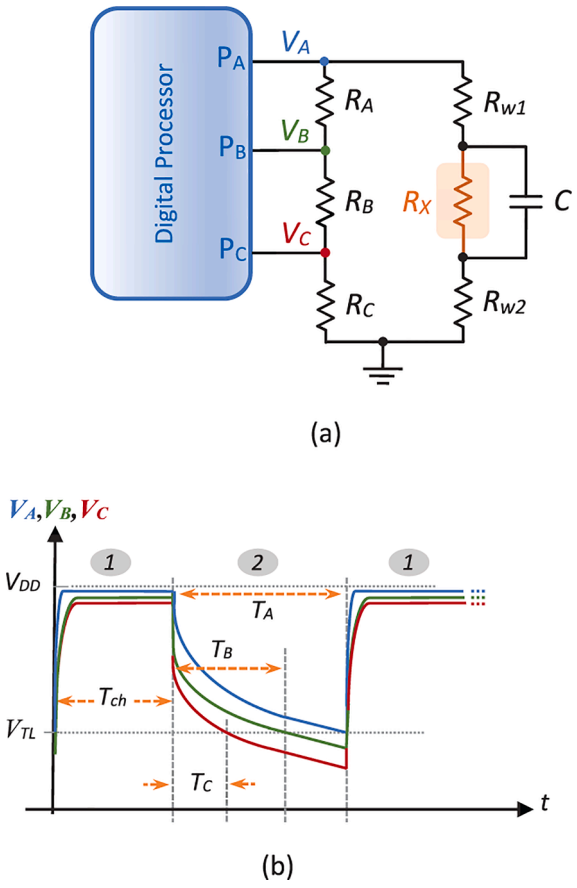

Fig. 4. (a) Proposed circuit to reduce uncertainty in the estimation of R_X (Improved Method). (b) Waveforms of $V_A(t)$, $V_B(t)$, and $V_C(t)$ following the steps described in Table II.

Table 2
Steps to obtain RX in the IM.

STEPS	STATE OF PINS		
	P_A	P_B	P_C
1 – Charging C	'1'	'1'	'1'
2 – Discharging C	'HZ'	'HZ'	'HZ'

As in the TMM, the three required time measurements, T_A, T_B, and T_C, are obtained during the *Discharging C* step. Since in the IM.

$$R_T = (R_A + R_B + R_C + R_w) \parallel R_X \tag{15}$$

these times are

$$T_A = R_T C \ln\left(\frac{V_A(0)}{V_{TL}}\right) = R_T C \ln\left(\frac{\Delta V_{Cap,\max} - I(0)\cdot R_w}{V_{TL}}\right) \tag{16}$$

$$T_B = R_T C \ln\left(\frac{V_B(0)}{V_{TL}}\right) = R_T C \ln\left(\frac{R_B + R_C}{R_A + R_B + R_C}\cdot\frac{\Delta V_{Cap,\max} - I(0)\cdot R_w}{V_{TL}}\right) \tag{17}$$

$$T_C = R_T C \ln\left(\frac{V_C(0)}{V_{TL}}\right) = R_T C \ln\left(\frac{R_C}{R_A + R_B + R_C}\cdot\frac{\Delta V_{Cap,\max} - I(0)\cdot R_w}{V_{TL}}\right) \tag{18}$$

Considering (16)-(18), an expression can be found to ascertain R_T in the IM:

$$R_T = \frac{T_A - (T_B + T_C)/2}{C\cdot\ln\left(\frac{R_A+R_B+R_C}{\sqrt{(R_B+R_C)R_C}}\right)} = k'(T_A - (T_B + T_C)/2) \tag{19}$$

where k' is the new constant to store in the DP:

$$k' = \frac{1}{C\cdot\ln\left(\frac{R_A+R_B+R_C}{\sqrt{(R_B+R_C)R_C}}\right)} \tag{20}$$

By averaging the time measurements with higher uncertainty, a more accurate value of R_T is obtained using (19) instead of (6). Furthermore, using (19) obtains a more accurate estimation of R_X^*:

$$R_X^* \approx \frac{1}{\frac{1}{R_T} - \frac{1}{R_A+R_B+R_C}} = \frac{k'(R_A + R_B + R_C)(T_A - (T_B + T_C)/2)}{R_A + R_B + R_C - k'(T_A - (T_B + T_C)/2)} \tag{21}$$

The IM performs the steps indicated in Table 2 for the circuit in Fig. 4 (a), obtaining the time measurements, T_A, T_B, and T_C, used in (21) to estimate R_X.

The relative error in the R_X estimation using (21) is the same as in (9), replacing $R_A + R_B$ with $R_A + R_B + R_C$. Meanwhile, following the same steps as in the TMM to calculate relative uncertainty, $u(R_X^*)/R_X^*$, obtains:

$$\frac{u(R_X^*)}{R_X^*} = \frac{\sqrt{\sum_i^{A,B,C}\left(\frac{\partial R_X^*}{\partial T_i}\right)^2 u^2(T_i)}}{R_X^*} \approx \frac{\sqrt{\sum_i^{A,B,C} u^2(T_i)}}{T_A - (T_B + T_C)/2} = \frac{\sqrt{\alpha_A^2 + (\alpha_B^2 + \alpha_C^2)/4}}{V_{TL}\cdot\ln\left(\frac{R_A+R_B+R_C}{\sqrt{(R_B+R_C)R_C}}\right)} \tag{22}$$

If $R_B \ll R_C$ is chosen in the IM, the denominator of the last member of (22) is practically equal to the denominator in (14). Also, $\alpha_C \approx \alpha_B$ since nodes B and C in Fig. 4 (a) are purely resistive. All this means that the relative uncertainty in R_X^* is lower in the IM than in the TMM. This improved R_X^* estimate comes at the cost of an additional measurement and resistor. Designers must take this increase in the complexity of the method into account when deciding whether to use the TMM or the IM. Section III includes a comparison of the results with both methods.

3. Experimental results and discussion

Given the flexibility these devices allow and their high

computational power, the proposed circuits have been designed choosing an FPGA as DP. The FPGA used is the Artix 7 XC7A35T from Xilinx (San Jose, CA) with a 50 MHz internal clock. The FPGA is integrated on a general-purpose CMOD-A7 board from Digilent (Pullman, WA), which can be connected to a laptop via a USB port. The rising and falling edges of the clock have been used to measure time. The counts of these times, therefore, increment every ten ns. The supply voltage of the pins in the FPGA are $V_{DD} = 3.3$ V and $V_{TL} = 1.26$ V, approximately.

The main blocks of the FPGA architecture are shown in Fig. 5. The configuration of the pins, the counter module, and the two or three registers that store the time measurements depend on the Control Unit. A USB communications module has been introduced to send the results obtained by the Arithmetic Unit to a laptop.

To have a set of measurements as a reference to evaluate errors in the TMM and the IM when introducing the lead wire resistances, a series of eighteen precision resistors in the range 100–2000 Ω has been selected along with resistors $R_{w1} = R_{w2} = 0$ Ω. This range includes a set of commercial RTDs (Pt100, Pt250, Pt1000, and Pt2000). To study the effects of the lead wire resistances on the TMM and the IM, 100, 250, 1000, and 2000 Ω resistors have been used in another series of tests to emulate RTDs, along with 2, 4, 6, 10, 15, 20, 30, 40, and 50 Ω resistors for R_{w1} and R_{w2}. Therefore, a total of 54 different tests were performed for the TMM and the IM. The capacitor used in all tests was 418.6 nF. Since this is an excessively high value for an NP0 capacitor, this capacitance has been obtained by placing several capacitors in parallel. $R_A = 4650.3$ Ω and $R_B = 10064$ Ω were selected for the TMM, and $R_A = 4340$ Ω, $R_B = 300$ Ω, and $R_C = 10064$ Ω for the IM. All resistance and capacitance values were measured with an Instek LCR-6300 m.

The choices of R_A, R_B, and R_C guarantee, firstly, that $V_B(0) > V_{TL}$ in the TMM and $V_C(0) > V_{TL}$ in the IM and, secondly, that $R_A + R_B$ in the IM practically equals R_A in the TMM. Thus, T_A and T_B in the TMM are very similar to T_A and T_C in the IM. Finally, as commented, by choosing $R_B \ll R_C$ the uncertainty in (22) is reduced compared to (14).

With these choices, the lowest count for T_B in the TMM is about 1000, corresponding to 10 μs, and the same for T_C in the IM (this occurs for $R_X = 100$ Ω). Quantization errors are, therefore, minor. The maximum measurement times correspond to T_A and are 706 μs (1.09 ms including charging time), for the TMM and the IM, with $R_X = 2000$ Ω and $R_w = 100$ Ω. Therefore, the maximum count value for T_A is around 70,600, and it is necessary to implement a 16-bit counter in the FPGA, together with a small circuit, to detect if the trigger instant has occurred with a high or low the system clock value. Fig. 6 shows R_X as a function of T_A - T_B for the TMM when $R_w = 0$ Ω and where T_A and T_B are the average

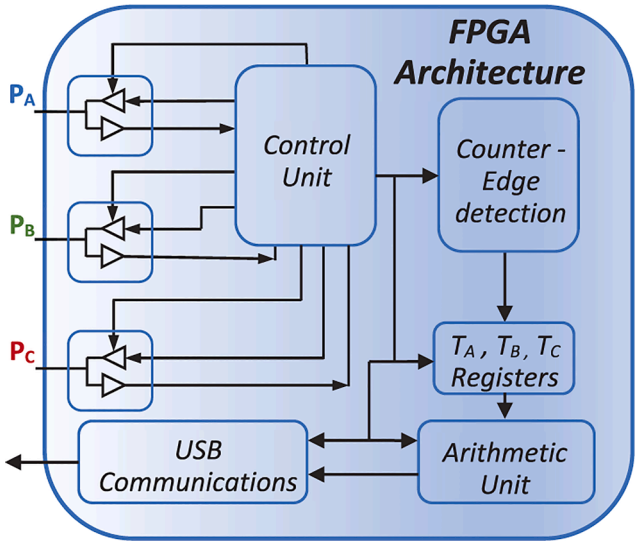

Fig. 5. The internal architecture programmed in the FPGA.

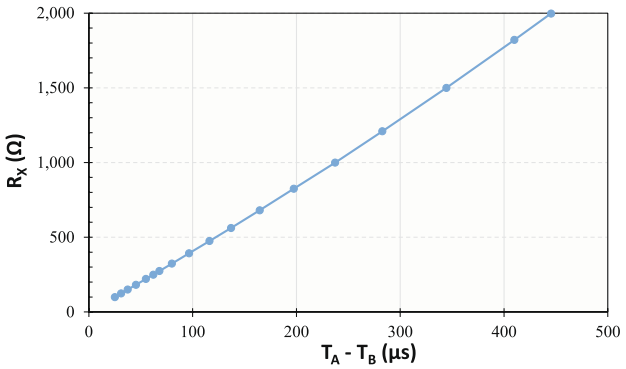

Fig. 6. R_X as a function of the experimental measures of T_A - T_B for the TMM.

values obtained in a set of two hundred R_X estimates. This figure shows good linearity between R_X and T_A - T_B as shown by (6).

These two hundred R_X estimates are made on each of the 54 tests to analyze various figures of merit. The first one is the maximum relative error for R_X*, e_R, given by.

$$e_R = \mathrm{Max}\left(\frac{\left|R_X^*(i) - R_{X,a}\right|}{R_{X,a}} \times 100\%\right); \quad i = \{1, 2, \ldots, 200\} \tag{23}$$

where R_X*(i) is each of the estimations of R_X using (8) or (21), and $R_{X,a}$ is the actual resistance value measured by the LCR meter. Another figure of merit is the systematic error, e_S, defined by.

$$e_S = \frac{\left|\overline{R} - R_{X,a}\right|}{R_{X,a}} \times 100\% \tag{24}$$

where $\overline{R}$ is the average of all R_X*(i). In our case, e_R and e_S include error when using R_X* as the estimation value. e_R and e_S are shown in Fig. 7 for the TMM with $R_X \in [100, 2000]$ Ω, and $R_w = 0$ Ω. e_R is always less than 0.2%, except for $R_X = 100$ Ω and $R_X = 124.4$ Ω. For e_S, the maximum is 0.12% for $R_X = 124.4$ Ω.

Trigger uncertainty in the time measurements is mainly responsible for the difference between e_R and e_S. To analyze the behavior of these uncertainties, Fig. 8 shows the relative time uncertainties $u(T_i)/(T_A - T_B)$. The results shown in Fig. 8 confirm the validity of (12), since the values are practically constant for both uncertainties. Also, it is confirmed that $u(T_B) > u(T_A)$ for any value of R_X. On average, the quotient $u(T_B)/u(T_A)$ takes a value of 1.41 for the whole R_X values range. Since uncertainties in the time measurements are approximately constant, the same should be valid for relative uncertainties $u(R_X^*)/R_X^*$, as shown by (14) and (22). For the TMM, this relative uncertainty can be obtained from the data in Fig. 7, considering that.

$$\frac{u\left(R_X^*\right)}{R_X^*} = \sqrt{e_R^2 - e_S^2} \tag{25}$$

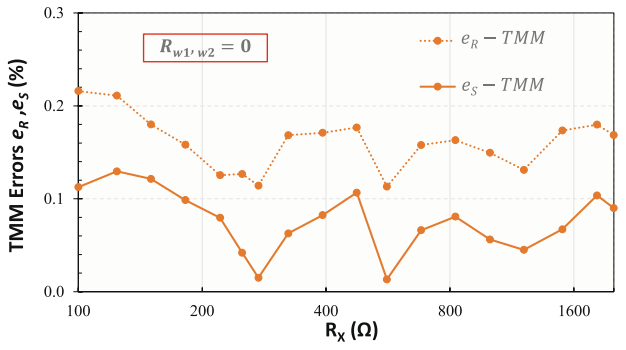

Fig. 7. Relative errors, e_R, and systematic errors, e_S, for the TMM in the estimation of R_X when $R_{w1} = R_{w2} = 0$.

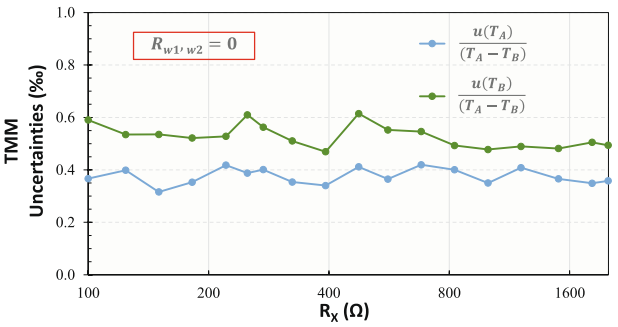

Fig. 8. Relative uncertainties in time measurements for the TMM.

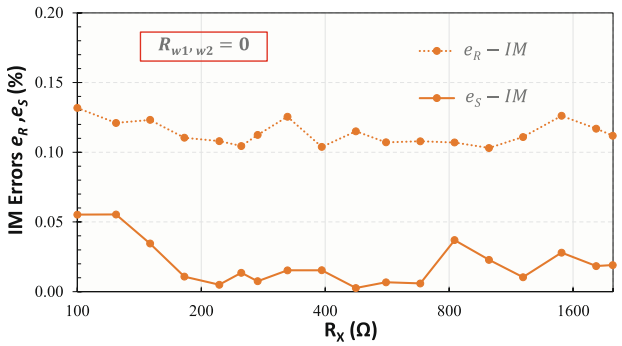

Fig. 9. Relative errors, e_R, and systematic errors, e_S, for the IM in the estimate of R_X when $R_{w1} = R_{w2} = 0$.

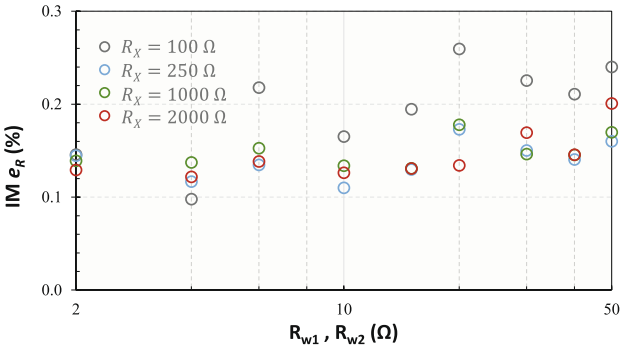

Fig. 10. e_R error for the IM with different R_{w1}, R_{w2}, and R_X values.

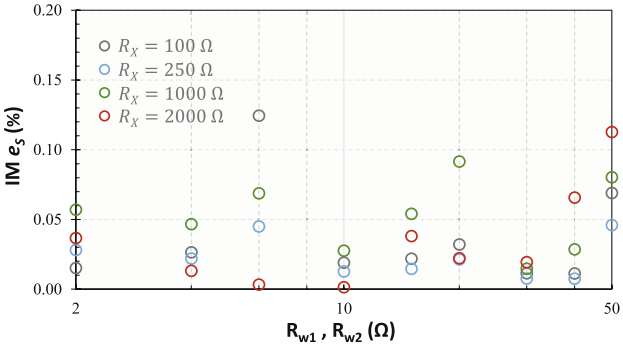

Fig. 11. e_S error for the IM with different R_{w1}, R_{w2}, and R_X values.

The values oscillate slightly around 0.13% with two maximums of 0.18% and 0.16% for $R_X = 100\ \Omega$ and $R_X = 124.4\ \Omega$, respectively. The increase in these cases is due to the small contribution of quantization uncertainty.

The introduction of R_{w1} should increase $u(T_A)$ because the A nodes of the TMM and IM circuits will no longer be directly connected to the capacitor. However, since the values of R_{w1} are small, so will the increments in $u(T_A)$. To check the effects of R_w on the $u(T_B)/u(T_A)$ ratio in the TMM circuit, its value was measured in the cases R_{w1}, $R_{w2} = 50\ \Omega$ and R_{w1}, $R_{w2} = 0\ \Omega$ for three values of R_X. The results are shown in Table 3. Although, in general, there is a slight reduction in the ratio, it is still the case that $u(T_B) > u(T_A)$.

These results indicate that the IM should show smaller errors than the TMM for any combination of R_X and R_w. Fig. 9 confirms this situation by showing the IM errors in situations analogous to those in Fig. 7 for the TMM. It is particularly noteworthy that e_S is also lower in the IM than in the TMM. Obviously, the reduction of e_S also translates into a reduction of e_R. However, using (25), it can be seen that $u(R_X^*)/R_X^*$ is also reduced, as expected, these being in the range of 0.10% − 0.11% in all cases. Thus, the reduction of e_R shown in Fig. 9 is, therefore, due to both a decrease of e_S and $u(R_X^*)/R_X^*$.

Figs. 10 and 11 show IM errors when non-zero R_w values are taken. In both figures, the X-axis shows the R_{w1} and R_{w2} values (in a logarithmic scale) equal for both resistors (although this is unnecessary for the method to work). The Y-axis shows the errors for different R_X values matched to several commercial RTDs. Figs. 10 and 11 show minimal variations in the errors compared to those shown in Fig. 9, showing the insensitivity of the estimations with R_w.

For $R_X = 100\ \Omega$, the errors show similar behavior to the other R_X values up to $R_{w1} = R_{w2} = 10\ \Omega$. For larger values of R_w, the error would increase significantly (not shown in Figs. 10 and 11). This behavior is because for such a small R_X resistance value, $\Delta V_{Cap,\max}$ is also small, and R_w above 10 Ω makes the initial value of V_A at the start of the discharge in the IM less than V_{TL}. As discussed, this can be solved by simply adding a small resistor in series with R_X between the C terminals when necessary. To show the results of Figs. 10 and 11, it has been decided to add a 50 Ω resistor in series with $R_X = 100\ \Omega$, if $R_w > 20\ \Omega$. It is important to note that, in practice, situations with $R_w > 20\ \Omega$ are hard to find. In any case, the maximum values of e_R and e_S using the IM are 0.26% and 0.12%, respectively (regardless of the value of R_X).

For the TMM, proceeding in the same way as for the IM, the maximum value for e_R is 0.29% and 0.15% for e_S. The results show graphs with shapes very similar to those of Figs. 10 and 11 (for this reason, they have not been added). The only difference is a general increase in errors of approximately 0.03%.

Table 3
Ratio $u(t_a)/u(t_b)$ in the TMM.

R_X (Ω)	R_{w1}, $R_{w2} = 0\ \Omega$	R_{w1}, $R_{w2} = 50\ \Omega$
250	1.573	1.506
1000	1.366	1.126
2000	1.379	1.188

4. Conclusions

A major problem in the digital readout of remote resistive sensors is the presence of resistances in the lead wires. This fact can increase errors in the sensor resistance estimation, R_X, especially if the resistance value is small, as in the case of resistance temperature detectors (RTD). This paper presents two novel proposals based on so-called direct interface circuits (DICs) to overcome this problem. The circuits are very simple, as the first proposal only requires two resistors and a capacitor (in addition to a digital processor) to obtain two time measurements to estimate R_X. The second proposal uses one more resistor, allowing a third time measurement that reduces the errors in estimating R_X. The arithmetic operations involved in the estimations are simply multiplications and subtractions, which can be easily implemented in the DP.

All time measurements are obtained during a single capacitor charging–discharging process. This saves time and power consumption

compared to other implementations requiring a larger number of such processes.

Experimental results have been obtained for R_X ranging from 100 to 2000 Ω with lead wire resistances ranging from 0 to 100 Ω. The maximum systematic errors are 0.15% for the first proposal and 0.12% for the second, with a maximum measurement time of 1.09 ms.

Declaration of Competing Interest

The authors declare that they have no known competing financial interests or personal relationships that could have appeared to influence the work reported in this paper.

Data availability

Data will be made available on request.

Acknowledgements

This work was supported by the Spanish Government under contract PID2021-125091OB-I00. Funding for open access charge: Universidad de Málaga / CBUA.

References

[1] J. W. Chuah, The internet of things: an overview and new perspectives in systems design, in: Proc. 14th Int. Symp. Integr. Circuits, ISIC 2014, 2015, pp. 216–219.
[2] M. Ganzha, M. Paprzycki, W. Pawłowski, P. Szmeja, K. Wasielewska, Semantic interoperability in the Internet of Things: an overview from the INTER-IoT perspective, J. Netw. Comput. Appl. 81 (2017) 111–124.
[3] F. Reverter, J. Jordana, M. Gasulla, R. Pallàs-Areny, Accuracy and resolution of direct resistive sensor-to-microcontroller interfaces, Sensors Actuators, A Phys. 121 (1) (2005) 78–87.
[4] J.A. Hidalgo-Lopez, Sigma-delta approach in direct interface circuits for readout of resistive sensors, IEEE Trans. Instrum. Meas. 71 (2022).
[5] K. Elangovan, S. Dutta, A. Antony, A.C. Sreekantan, Performance verification of a digital interface suitable for a broad class of resistive sensors, IEEE Sens. J. 20 (23) (2020) 13901–13909.
[6] Z. Czaja, A measurement method for capacitive sensors based on a versatile direct sensor-to-microcontroller interface circuit, Meas. J. Int. Meas. Confed. 155 (2020), 107547 (October 2020).
[7] O. Lopez-Lapeña, E. Serrano-Finetti, O. Casas, Calibration-less direct capacitor-to-microcontroller interface, Electron. Lett. 52 (4) (2016) 289–291.
[8] J.A. Hidalgo-López, J. Castellanos-Ramos, Simplifying capacitive sensor readout using a new direct interface circuit, IEEE Trans. Instrum. Meas. (2022), 1.
[9] A. Asif, A. Ali, M.Z.U. Abdin, Resolution enhancement in directly interfaced system for inductive sensors, IEEE Trans. Instrum. Meas. 68 (10) (2018) 4104–4111.
[10] T.K. Maiti, A. Kar, Novel remote measurement technique using resistive sensor as grounded load in an opamp based V-to-I converter, IEEE Sens. J. 9 (3) (2009) 244–245.
[11] W. Petchmaneelumka, P. Julsereewong, A. Julsereewong, J. Tongpakpanang, Simple interface circuit with lead-wire-resistance compensation for single resistive sensors, Int. Conf. Control. Autom. Syst. (2012) 1076–1079.
[12] A. Rerkratn, S. Prombut, T. Kamsri, V. Riewruja, W. Petchmaneelumka, A procedure for precise determination and compensation of lead-wire resistance of a two-wire resistance temperature detector, Sensors 22 (11) (2022).
[13] P. Julsereewong, A. Julsereewong, A. Rerkratn, N. Pootharaporn, Simple resistance-to-time converter with lead-wire-resistance compensation, 2011, pp. 2760–2763.
[14] R. Anandanatarajan, U. Mangalanathan, U. Gandhi, Enhanced microcontroller interface of resistive sensors through resistance-to-time converter, IEEE Trans. Instrum. Meas. 69 (6) (2020) 2698–2706.
[15] G. Singh, G. S. Member, U. Mangalanathan, U. Gandhi, S. Sohail, Improved resistance to digital converter for low-value resistive sensor with lead wire compensation, 2022, pp. 1–6.
[16] L. Wei, X. Shusheng, Z. Xiaojun, Lead-wire-resistance compensation technique, Sensors 20 (2020), 2742.
[17] P.R. Nagarajan, B. George, V.J. Kumar, Improved single-element resistive sensor-to-microcontroller interface, IEEE Trans. Instrum. Meas. 66 (10) (2017) 2736–2744.
[18] K. Elangovan, A.C. Sreekantan, Evaluation of new digital signal conditioning techniques for resistive sensors in some practically relevant scenarios, IEEE Trans. Instrum. Meas. 70 (2021).
[19] K. Elangovan, A. Antony, A. Chandrika Sreekantan, Simplified digitizing interface-architectures for three-wire connected resistive sensors: design and comprehensive evaluation, IEEE Trans. Instrum. Meas. 71 (2022).
[20] F. Reverter, A microcontroller-based interface circuit for three-wire connected resistive sensors, IEEE Trans. Instrum. Meas. (2022).
[21] F. Reverter, M. Gasulla, R. Pallas-Areny, R. Pallàs-Areny, Analysis of power-supply interference effects on direct sensor-to-microcontroller interfaces, IEEE Trans. Instrum. Meas. 56 (1) (2007) 171–177.
[22] J.A. Hidalgo-López, Ó. Oballe-Peinado, J. Castellanos-Ramos, J.C. Tejero-Calado, F. Vidal-Verdú, Wide range calibration method for direct interface circuits and application to resistive force sensors, IEEE Sens. J. 21 (20) (2021) 22956–22966.